This work was carried out by the Sustainable Materials Chemistry Group at the University of Paderborn (Germany), in collaboration with Xiangtan University and Hebei University of Science and Technology (China).

Tin chloride metal salt modified carbon nitride for efficient hydrogen and hydrogen peroxide production from pure water *via* piezocatalysis

Using a molten $SnCl_2$ salt strategy, defect-engineered carbon nitride/Sn composites were developed for efficient piezocatalytic hydrogen and hydrogen peroxide production directly from pure water under ultrasonication, without sacrificial agents or noble metals.

Image reproduced by permission of Maria de las Nieves López-Salas from *J. Mater. Chem. A*, 2026, **14**, 8575.

As featured in:

See Ying Pan, Ran Su, Nieves López-Salas *et al.*, *J. Mater. Chem. A*, 2026, **14**, 8575.

ROYAL SOCIETY OF CHEMISTRY

rsc.li/materials-a

Registered charity number: 207890

Journal of Materials Chemistry A

ROYAL SOCIETY OF CHEMISTRY

PAPER

View Article Online
View Journal | View Issue

Cite this: J. Mater. Chem. A, 2026, 14, 8575

Tin chloride metal salt modified carbon nitride for efficient hydrogen and hydrogen peroxide production from pure water *via* piezocatalysis

Ying Pan, *[a] Luocheng Liao,[b] Dan Qiao,[a] Irene Lamata Bermejo,[a] Yunya Liu, [b] Ran Su*[c] and Nieves López-Salas *[a]

Received 26th September 2025
Accepted 26th January 2026

DOI: 10.1039/d5ta07919e

rsc.li/materials-a

Piezocatalysis presents a sustainable and energy-efficient method for producing hydrogen (H_2) and hydrogen peroxide (H_2O_2), utilizing mechanical energy to drive chemical reactions without the need for external power sources or harmful chemicals. In this study, we used a one-pot synthetic method to modify graphitic carbon nitride (g-C_3N_4). The obtained catalysts showed enhanced H_2 and H_2O_2 production from pure water without any co-catalysts or sacrificial agents *via* piezocatalysis. In the cost-effective synthetic method, a metal oxide/g-C_3N_4 composite structure was constructed through the molten salt method. During thermal pyrolysis, non-noble metal-based $SnCl_2$ provided a molten medium to facilitate the exfoliation of the g-C_3N_4 layer. The oxidation of $SnCl_2$ and its interaction with g-C_3N_4 promoted the formation of g-C_3N_4/Sn-based composites. The synergistic interaction between exfoliated, defect-rich g-C_3N_4 and non-piezoelectrically active Sn species leads to a significant enhancement of the piezoelectric effect compared to pristine g-C_3N_4. Notably, the g-C_3N_4/Sn-based composites achieved superior H_2 (3846.46 μmol g^{-1} h^{-1}) and H_2O_2 (999.11 μmol g^{-1} h^{-1}) production rates from pure water. This work provides new insights into the structural and compositional modulation of g-C_3N_4 without the use of any noble metals and paves the way for further piezocatalytic research using two-dimensional carbon nitride materials.

Introduction

Hydrogen (H_2), with its high energy density and clean combustion that yields only water, represents a promising alternative for mitigating CO_2 emissions. As a result, the production of H from water has become a key objective in the pursuit of low-carbon energy technologies.[1] In parallel, hydrogen peroxide (H_2O_2) is a widely used green oxidant in synthesis, disinfection, and bleaching. It has also gained attention as a potential fuel cell energy carrier. Direct synthesis of H_2O_2 from oxygen and water has attracted significant attention for its simplicity, safety, and lower energy demands.[2] Given the environmental and practical benefits of both H_2 and H_2O_2, as well as the inherent sustainability of using water as a feedstock, there is growing interest in developing green and efficient methods for their production. In particular, strategies that enable the generation of H_2 or H_2O_2 from water under mild conditions, without the use of noble metals or hazardous reagents, are highly desirable for advancing sustainable energy and chemical manufacturing.

The piezocatalytic properties of dielectric materials have recently attracted attention as a novel approach to energy conversion.[3,4] When subjected to mechanical vibration, these materials generate an internal electric field due to their non-centrosymmetric crystal structures, which drives the separation of electrons and holes and enables catalytic activity. In 2010, Xu and co-workers first demonstrated piezocatalytic water splitting,[5] showing that ZnO microfibers and $BaTiO_3$ microdendrites dispersed in water under ultrasonication could produce H_2 and O_2.[5] Unlike conventional systems that rely on metal redox reactions, these piezocatalysts generate strain-induced charge carriers without undergoing chemical changes.[6] Since then, researchers have been rigorously expanding this field by focusing either on piezocatalyst design or on combining piezocatalysis with other catalytic techniques. In terms of catalyst design, most studies have concentrated on the following types of piezoelectric materials, such as ZnO,[5] perovskites,[6] two-dimensional transition metal sulfides/selenides,[7] layered bismuth-based piezoelectrics,[8] and their composites.[9,10] With respect to catalytic reactions, most researchers have focused on piezo-assisted photocatalysis.[11,12] Great improvement has been achieved in this field.[13] However,

[a]Department of Chemistry, University of Paderborn, Paderborn 33098, Germany. E-mail: ying.pan@uni-paderborn.de; nieves.lopez.salas@uni-paderborn.de

[b]Key Laboratory of Low Dimensional Materials and Application Technology of Ministry of Education, School of Materials Science and Engineering, Xiangtan University, Xiangtan 411105, China

[c]Hebei Key Laboratory of Photoelectric Control on Surface and Interface, College of Science, Hebei University of Science and Technology, Shijiazhuang 050018, China. E-mail: suranxida@163.com

the efficiency of pure piezoelectric water splitting for H_2 production remains much lower than that of established methods like photocatalysis.[14] To realize the full potential of this approach, further advancements are needed in the design and development of materials with enhanced piezoelectric properties and catalytic performance under mechanical vibration.

Graphitic carbon nitride (g-C_3N_4), a metal-free polymeric material composed primarily of earth-abundant carbon and nitrogen, has attracted growing interest in piezocatalytic applications. This interest stems from its inherent flexoelectricity and the presence of nanoscale, triangular-shaped, non-centrosymmetric holes that contribute to its piezoelectric behavior.[15] Moreover, the conjugated ring structure of g-C_3N_4 provides abundant pyridinic nitrogen sites, which have been identified as active centers for oxygen adsorption and activation.[16,17] In 2019, Wang and co-workers reported the first example of H_2O_2 production from water and oxygen *via* piezocatalysis using g-C_3N_4, achieving a rate of 34 μmol h^{-1} at an ultrasonic frequency of 53 kHz without the use of scavengers.[18] g-C_3N_4 exhibits inherently lower piezoelectric efficiency compared to conventional metal-based dielectric materials. Structural modification through the introduction of carbon and nitrogen vacancies has been proposed as a strategy to disrupt symmetry in the g-C_3N_4 lattice, thereby enhancing its piezoelectric response. However, the observed enhancement remains limited, and current modification strategies are largely restricted to liquid-phase or thermal exfoliation methods.[19]

Molten salt methods have been extensively employed to modify carbon-based materials, particularly in applications such as gas adsorption and energy storage.[20] These salt melts provide a liquid media that facilitate the condensation and aromatization of organic precursors at temperatures beyond the capabilities of conventional solvents. Additionally, molten salts can function as structure-directing or templating agents, enabling fine-tuning of the microstructure across a wider range of conditions.[21] In contrast to thermally polycondensed melon-type carbon nitride, which is typically amorphous or poorly crystalline, molten salts enhance mass and energy transport during thermal treatment, thereby promoting more efficient recondensation processes.[22] Recently, Odziomek and co-workers introduced $SnCl_2$ as a non-innocent molten salt medium for synthesizing nanoporous carbons.[23] With its low melting point, $SnCl_2$ serves as a solvent, significantly influencing the development of porosity in the resulting materials.

In this study, we combined the unique properties of g-C_3N_4 with the advantages of the $SnCl_2$-based molten salt method to synthesize a one-pot modified g-C_3N_4 composite anchored with Sn-based species. To the best of our knowledge, this work is the first to report the use of reactive $SnCl_2$ salt methods to modify g-C_3N_4 to enhance its piezoelectric effect for catalytic applications. During the thermal pyrolysis process, $SnCl_2$ acts similarly to conventional molten salt methods, promoting the exfoliation of g-C_3N_4 layers. Additionally, the oxidation of $SnCl_2$ and its interaction with g-C_3N_4 facilitate the formation of g-C_3N_4/Sn-based composites. These composites exhibit a significantly enhanced piezoelectricity compared to pure g-C_3N_4. Notably, the g-C_3N_4/Sn-based composites demonstrate superior H_2 and H_2O_2 production rates from pure water. This work provides valuable insights into the structural and compositional modulation of g-C_3N_4 and may inspire further studies on piezocatalytic applications of two-dimensional carbon nitride-based materials.

Results and discussion

Morphology and structure

As illustrated in Fig. 1a, carbon nitride–metal oxide composites were synthesized *via* a thermal treatment process involving the mixing of melamine with $SnCl_2$ salt, followed by calcination at 500 °C. Depending on the atmosphere employed during thermal treatment, two different samples were obtained: M-

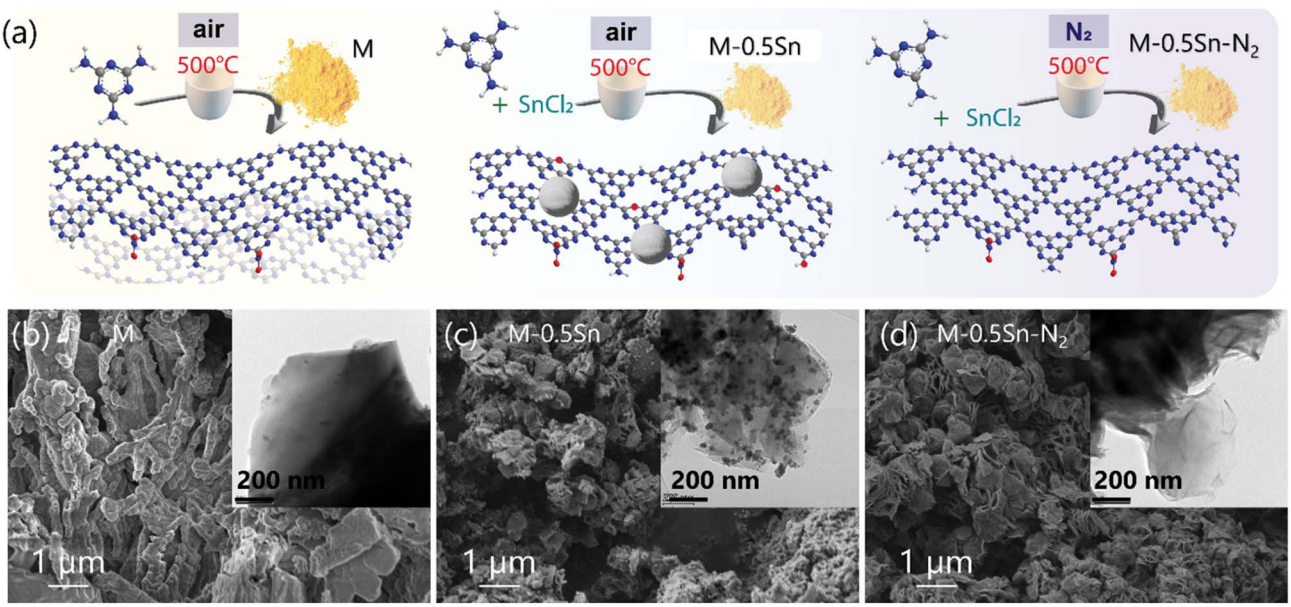

Fig. 1 (a) Illustration of the sample preparation process; The SEM and TEM (insert) morphologies of (b) M, (c) M-0.5Sn, and (d) M-0.5Sn–N_2.

0.5Sn (air atmosphere) and M-0.5Sn–N_2 (nitrogen atmosphere). For comparison, pristine g-C_3N_4 (denoted as M) was also prepared in the absence of $SnCl_2$. Detailed synthesis procedures are provided in the Experimental section. The morphologies of the resulting samples were characterized using scanning electron microscopy (SEM) and transmission electron microscopy (TEM), as shown in Fig. 1 and S1. Pristine g-C_3N_4 (M) exhibited a bulk, layered structure (Fig. 1b). In contrast, both M-0.5Sn (Fig. 1c) and M-0.5Sn–N_2 (Fig. 1d) displayed significantly thinner, exfoliated nanosheet structures. This suggests that $SnCl_2$ facilitates the exfoliation of g-C_3N_4 during pyrolysis, leading to a marked reduction in layer thickness. In samples treated under air (M-0.5Sn), small particles were observed on the surface of the exfoliated sheets (Fig. 1c). The EDS results confirm the presence of C, N, O, and Sn elements. The Sn element is mainly distributed within Sn-containing nanoparticles (Fig. S1), which are anchored on the surface of the g-C_3N_4 nanosheets, consistent with the TEM image shown in Fig. 1c (inset). Both the quantity and agglomeration of these particles increased with higher $SnCl_2$ loading (Fig. S1a–d). In contrast, the sample prepared under a nitrogen atmosphere (M-0.5Sn–N_2) maintained an exfoliated morphology but showed no detectable particle formation (Fig. 1d), suggesting that metal particles are formed only under oxidative conditions.

An additional sample (M-0.5KSn) was synthesized using a KCl–$SnCl_2$ mixture instead of $SnCl_2$ alone to further investigate the role of metal salt composition. As shown in Fig. S2e and f, M-0.5KSn also exhibited an exfoliated morphology relative to pristine g-C_3N_4, but the layers were thicker compared to M-0.5Sn. This indicates that the KCl–$SnCl_2$ mixture has a weaker exfoliating effect and may also suppress the oxidation of metal salts to some extent. This can be explained by the formation of compounds in the system KCl–$SnCl_2$. Elemental compositions of the samples were analyzed *via* inductively coupled plasma (ICP) spectroscopy. As summarized in Table S1, samples treated under air contained significant amounts of residual Sn, whereas M-0.5Sn–N_2 showed only trace levels. These results can be explained as follows. Under an N_2 atmosphere, no oxidation occurs, and the molten salt acts solely as an exfoliating medium, converting melamine into g-C_3N_4. Most of the $SnCl_2$ is removed during the subsequent acid washing step. In contrast, under air, $SnCl_2$ not only serves as a molten medium to promote melamine decomposition and exfoliation but is also oxidized to form Sn-based oxides. These Sn-based nanoparticles cannot be readily removed by the 1 M HCl solution used in the experimental procedure, leading to the formation of Sn-based/g-C_3N_4 composites.

The crystal structures of the samples were characterized by X-ray diffraction (XRD). As shown in Fig. 2a, the pristine g-C_3N_4 sample (M) exhibits two characteristic diffraction peaks at 2θ = 13.1° and 27.3°. The weak peak at 13.1° corresponds to the in-plane structural packing of the tri-*s*-triazine units, indexed as the (100) reflection, while the strong peak at 27.3° is attributed to the interlayer stacking of conjugated aromatic systems, corresponding to the (002) reflection typically observed in graphitic materials. These features are consistent with the known crystal structure of g-C_3N_4.[24] In the case of M-0.5Sn–N_2, both peaks are present but with significantly reduced intensity, particularly for the (100) reflection, suggesting a loss of in-plane structural order due to increased distortion of the heptazine framework. Additionally, a slight shift of the (002) peak to higher angles was observed, indicating a reduction in interlayer spacing in the remaining crystallites, likely due to enhanced interlayer interactions or compression of the graphitic layers.[25–27] Notably, no additional diffraction peaks corresponding to Sn-containing phases were detected, suggesting the absence of crystalline Sn-based species. This observation is consistent with the SEM (Fig. 1d) and ICP (Table S1) results, which show no evidence of residual metal particles or significant Sn content in M-0.5Sn–N_2.

The XRD pattern of M-0.5Sn shows the disappearance of the characteristic g-C_3N_4 peaks at 13.1° and 27.3°, which is not only due to the exfoliation effect but can also be attributed to the emergence of new sharp peaks. These sharp peaks correspond to Sn_3O_4, SnO_2, and unreacted $SnCl_2$ (Fig. S3). The presence of Sn_3O_4 and SnO_2 indicates that $SnCl_2$ underwent partial oxidation during calcination under an air atmosphere, while the residual $SnCl_2$ likely results from incomplete oxidation and its limited solubility, which hinders complete removal during post-synthesis washing.[28,29] For the M-0.5KSn sample, no diffraction peaks

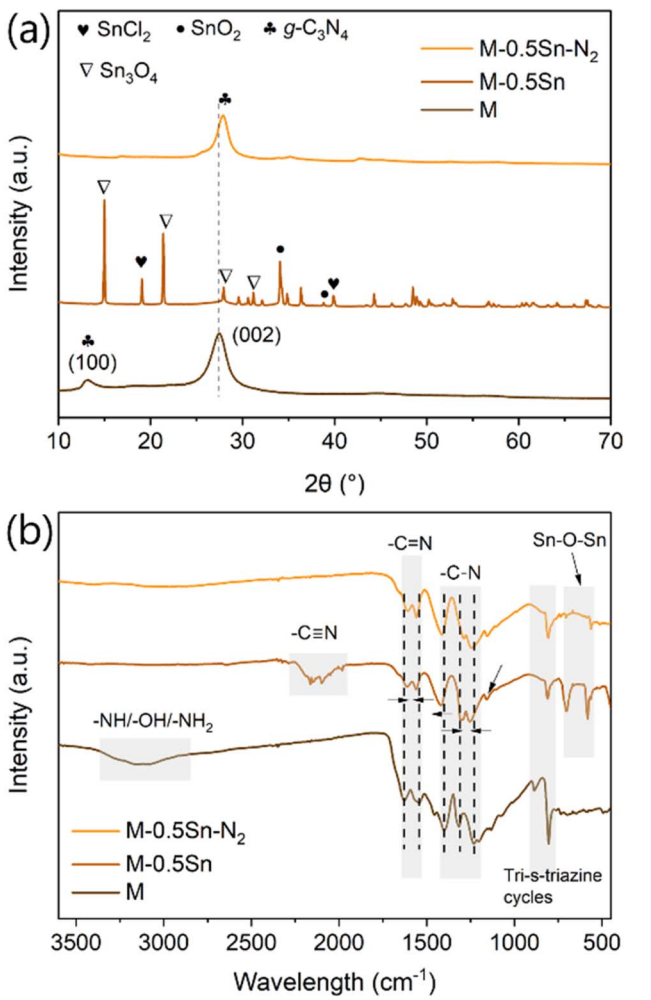

Fig. 2 (a) XRD patterns and (b) FTIR patterns of the samples.

corresponding to KCl were observed (Fig. S4a), suggesting that the interaction with g-C_3N_4 primarily involves Sn-containing species rather than KCl. Furthermore, reducing the $SnCl_2$-to-melamine ratio in the precursor mixture led to a decrease in the intensity and number of Sn-related peaks (Fig. S5a), consistent with the lower $SnCl_2$ content in the reaction system.

The Fourier transform infrared (FT-IR) spectra offered valuable insights into the chemical structures of the various samples (Fig. 2b). All samples displayed characteristic vibrational bands near 800 cm^{-1} and within the 1200–1700 cm^{-1} range, which are associated with the stretching vibrations of tri-*s*-triazine rings and C–N heterocycles, respectively.[30] Notably, the intensity of the band around 800 cm^{-1} was significantly reduced in the $SnCl_2$-treated samples compared to M, indicating a higher degree of structural disorder or defects within the carbon nitride framework. A distinct absorption peak at approximately 2180 cm^{-1} corresponding to the stretching vibration of cyanide (-C≡N) groups was observed in M-0.5Sn (Fig. 2b) as well as in other samples subjected to oxidative treatment (Fig. S4b and S5b). The presence of this peak is indicative of terminal –C≡N groups resulting from incomplete condensation, and it reflects an increased level of structural defects.[31] Broad absorption bands in the 2900–3600 cm^{-1} region were clearly visible in sample M, which can be attributed to surface-NH_x functionalities and physically adsorbed water molecules. In M-0.5Sn and M-0.5Sn–N_2, the bands within the 1200–1700 cm^{-1} region exhibited slight shifts relative to M, likely due to strong interactions between Sn-based species and aromatic C–N structures. The $SnCl_2$-treated samples showed new peaks (Fig. 2b and S5b) in the 570–700 cm^{-1} region, which are assigned to Sn–O–Sn stretching vibrations. In contrast, M-0.5Sn–N_2 exhibited only a weak single peak in this region, suggesting a significantly lower content of residual Sn species. This observation is consistent with other characterizations, including XRD, SEM, and ICP analyses.

X-ray photoelectron spectroscopy (XPS) was performed to further confirm the structures of the samples (Fig. 3). The survey spectrum (Fig. 3f) confirms the presence of O, N, and C elements in all three samples, with Sn as an additional element in M-0.5Sn. It should be noted that additional minor peaks are observed for the M-0.5Sn–N_2 sample, which can also be attributed to Sn-related signals (Fig. 3f). However, these peaks are generally not suitable for quantitative analysis or for distinguishing the chemical states of Sn, as they exhibit relatively weak intensities and small chemical shifts among different Sn oxidation states. Moreover, they are often affected by overlapping Auger features or background contributions. Fig. 3a shows the high-resolution C 1s spectra of the samples. Four peaks at a binding energy of 284.9, 286.5, 288.2, and 293.6 eV are assigned to C=C(C–C), –C≡N, N=C–N, and π excitation of heptazine rings, respectively.[21] We calculated the relative

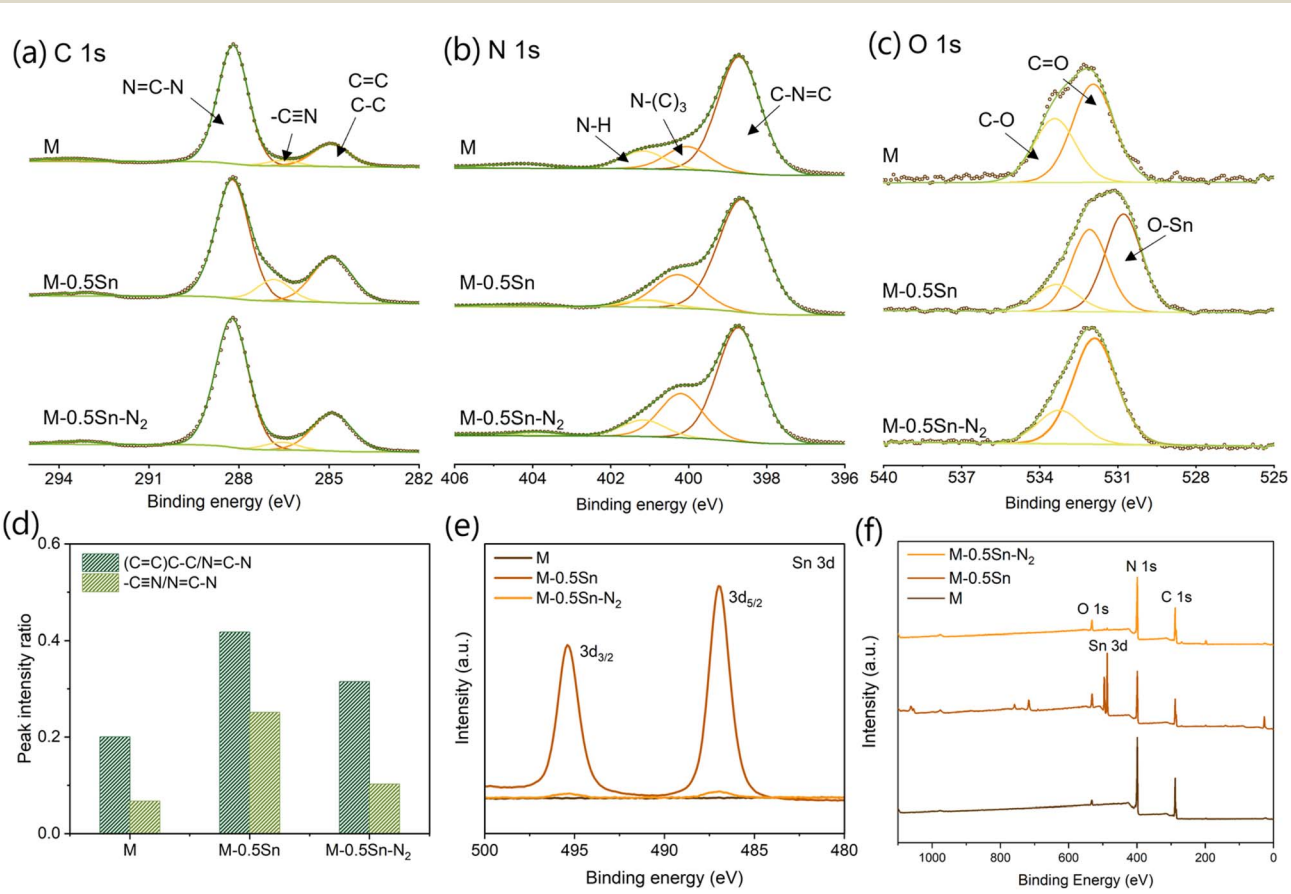

Fig. 3 High-resolution XPS spectra of (a) C 1s, (b) N 1s, and (c) O 1s for M, M-0.5Sn, and M-0.5Sn–N_2. (d) The peak intensity ratios of different N-containing bonds: data derived from (a). (e) High-resolution XPS spectra of Sn 3d, and (f) survey scan of all the samples.

peak intensity ratios to show the structure variations in different samples. As quantified in Fig. 3d, M shows the lowest ratio of the C=C(C–C) peak and the –C≡N peak, whereas M-0.5Sn shows the highest ratio for these two peaks among the three samples. The relative intensity of these two peaks indicates the degree of defect in the carbon nitride framework. These results prove that the oxidation of metal salts during sample preparation introduces more defects into the carbon nitride framework, which is well aligned with the FTIR analysis. Fig. 3b shows the high-resolution N 1 s spectra. The binding energies centered at 398.7, 400.1, and 401.2 eV can be ascribed to the C–N=C, N-$(C)_3$, N–H, and π excitation of heptazine rings, respectively.[31,32] While the binding energy of various N species in metal salt-treated samples remains largely unchanged compared to M, the relative peak intensity ratios of N-$(C)_3$ and N–H increase and decrease, respectively. This variation in the chemical environment is attributed to the modification induced by the Sn species. Fig. 3c shows the high-resolution O 1s spectra. One extra peak assigned to O–Sn was detected in M-0.5Sn compared to M and M-0.5Sn–N_2. Fig. 3e presents the high-resolution XPS spectra of Sn 3d, in which two distinct peaks are clearly attributed to Sn^{2+}/Sn^{4+} species.[33,34] The intensity of the Sn 3d peaks increases markedly when the samples are prepared under an oxidative atmosphere, consistent with the observations from SEM, XRD, and FTIR analyses.

Piezocatalytic performance

To investigate the role of Sn species in enhancing piezocatalytic activity, the piezocatalytic water splitting performance of various samples was evaluated in an ultrasonication bath (80 W, 40 kHz) without the use of any sacrificial agents or cocatalysts. As shown in Fig. 4a, the amount of H_2 produced increased progressively with ultrasonication time within each cycle. Moreover, M-0.5Sn demonstrated excellent stability over four consecutive cycles. The good stability of this catalyst was further confirmed by the negligible changes in its chemical structure before and after the reaction, as evidenced by the FTIR (Fig. S6a), XRD (Fig. S6b), and XPS (Fig. S7) results. Among the tested samples, M-0.5Sn exhibited the highest H_2 production rate, achieving 3846.46 μmol g^{-1} within one hour of ultrasonication: approximately 12 times greater than that of M (328.73 μmol g^{-1}) and about 8 times greater than that of M-0.5Sn–N_2 (456.79 μmol g^{-1}) (Fig. 4b). Although the exfoliation effect induced by $SnCl_2$ led to a significant reduction in the thickness of the g-C_3N_4 layers, sample M showed only a marginal increase in H_2 production. This indicates that the mere thinning of the g-C_3N_4 layers does not substantially enhance piezocatalytic performance. To further elucidate the origin of the performance enhancement observed in M-0.5Sn, the influence of varying $SnCl_2$ content on the piezocatalytic H_2 generation was investigated (Fig. 4c). While M-0.5Sn exhibited optimal activity, increasing the $SnCl_2$ content to produce M-1.0Sn led to a decline in H_2 evolution. This decrease is attributed to the excessive deposition of Sn-based nanoparticles, which excessively cover the carbon nitride nanosheets (Fig. S2c and d) and hinder their catalytic activity, as neither SnO_2 nor $SnCl_2$ typically exhibits any intrinsic piezoelectric properties.[13]

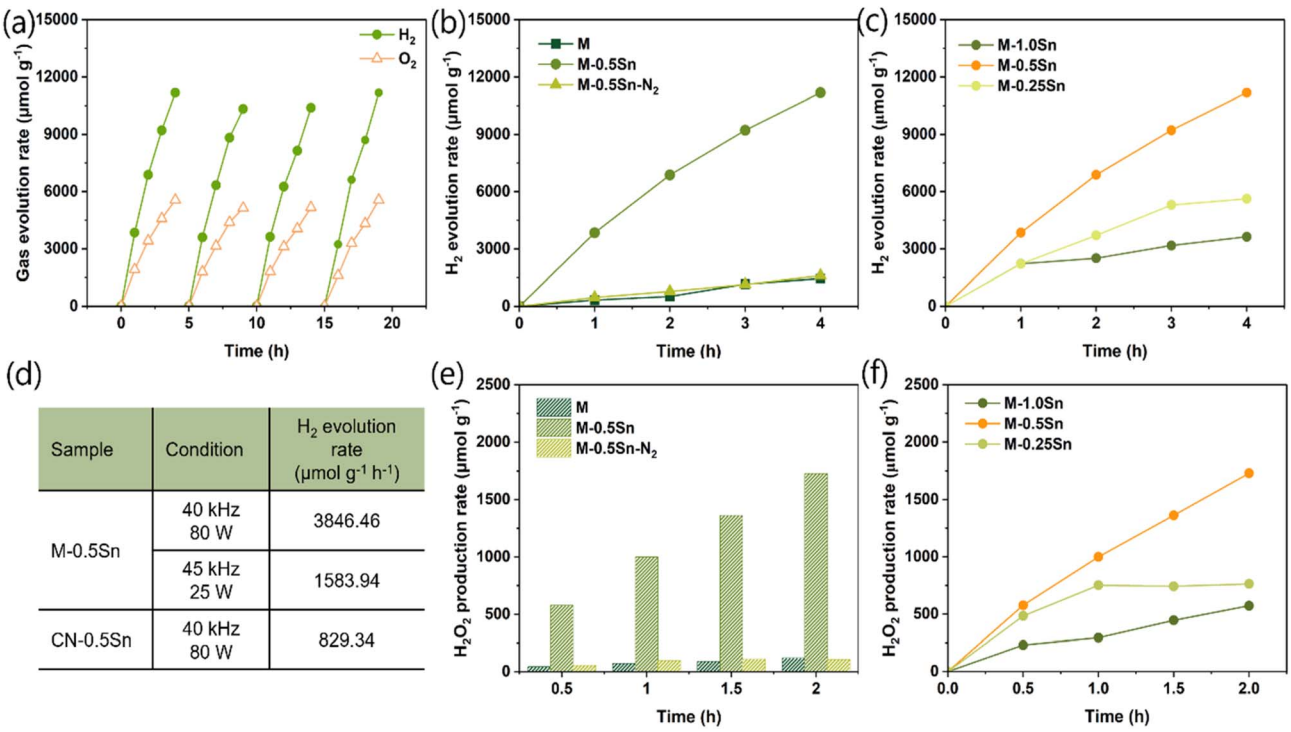

Sample	Condition	H_2 evolution rate (μmol g^{-1} h^{-1})
M-0.5Sn	40 kHz 80 W	3846.46
	45 kHz 25 W	1583.94
CN-0.5Sn	40 kHz 80 W	829.34

Fig. 4 (a) Recycling piezocatalytic H_2 evolution rates of M-0.5Sn. (b) H_2 evolution of M, M-0.5Sn, and M-0.5Sn–N_2, respectively. (c) Comparison of the H_2 evolution rate of M-1.0Sn, M-0.5Sn, and M-0.25Sn, respectively. (d) Comparison of the H_2 evolution rate of different samples at different reaction conditions. (e) H_2O_2 evolution rate of M, M-0.5Sn, and M-0.5Sn–N_2, respectively. (f) Comparison of the H_2O_2 evolution rate of M-1.0Sn, M-0.5Sn and M-0.25Sn, respectively.

To better understand the role of the interaction between g-C_3N_4 and Sn species, a comparative sample, CN-0.5Sn, was prepared by pyrolysing the mixture of $SnCl_2$ and the pre-synthesised g-C_3N_4 (Fig. S8). As shown in Fig. 4d, CN-0.5Sn exhibited a hydrogen production rate of 829.34 μmol g^{-1}, which is approximately twice that of the pristine g-C_3N_4 sample (M) but still significantly lower than that of M-0.5Sn. These results indicate that while the oxidation of $SnCl_2$ in contact with pre-formed g-C_3N_4 can moderately improve piezocatalytic performance, the enhancement is substantially more effective when Sn species are introduced during the precursor stage, likely due to stronger interfacial interactions and more uniform distribution within the g-C_3N_4 matrix. We also investigated the piezocatalytic reaction under two different ultrasonication baths available in the lab: 40 kHz–80 W and 45 kHz–25 W. The H_2 production rate decreased with decreasing ultrasonic power. This behavior can be attributed to the fact that higher ultrasonic power induces greater mechanical deformation and generates a stronger internal electric field, which enhances carrier separation and, consequently, improves catalytic performance. The superior performance of our optimal catalyst is further compared with previously published results in Table S2. As shown, M-0.5Sn exhibits comparable or even higher activity than the values reported in the literature. However, we also note that the ultrasonication conditions employed in these studies are not identical. Therefore, a more accurate comparison that considers the influence of ultrasonic energy is necessary for a more standardized evaluation in future work.

To investigate the influence of the Sn-g-C_3N_4 interaction on the piezoelectric response, the piezoelectric current responses of M, M-0.5Sn, and M-0.5Sn–N_2 were measured under periodic ultrasonic vibration. As shown in Fig. 5a, all three samples exhibit a pronounced and rapid increase in current upon ultrasonication, confirming the generation of piezo-induced charge carriers in the electrodes. Notably, M-0.5Sn shows a significantly enhanced piezoelectric polarization current compared with M and M-0.5Sn–N_2, indicating more efficient charge separation and transfer.[8,11,12] To further investigate the piezoelectric properties, the ferroelectric switching behaviour of M, M-0.5Sn, and CN-0.5Sn was examined using switching spectroscopy piezo response force microscopy (SSPFM). As shown in Fig. 5b and c, all three samples exhibited a complete 180° phase reversal (Fig. 5b) and a characteristic butterfly-shaped amplitude curve (Fig. 5c), confirming typical ferroelectric switching behaviour. Notably, the calibrated effective piezoelectric coefficient followed the trend: M-0.5Sn > M ≈ CN-0.5Sn. These findings suggest that the strong interaction between the Sn species and the carbon nitride framework formed during the pyrolysis of melamine in the presence of $SnCl_2$ is critical for enhancing piezoelectric performance.

The melting and oxidation of $SnCl_2$ during synthesis play a pivotal role in this enhancement. SnO_2 does not exhibit intrinsic ferroelectric behaviour. However, it can be integrated with ferroelectric materials, such as in heterostructures with $BaTiO_3$–TiO_2, which enhances specific ferroelectric properties in the resulting composite.[35] In this work, $SnCl_2$ serves a dual function: it facilitates the exfoliation of bulk g-C_3N_4 layers, and it introduces additional structural defects into the g-C_3N_4 matrix. Simultaneously, the oxidative atmosphere promotes the formation of Sn–O bonds during synthesis. The resulting Sn-based nanoparticles not only increase the specific surface area but also chemically interact with the g-C_3N_4 framework. Ultrasonic excitation induces periodic mechanical strain in the tin oxide/g-C_3N_4 composites, generating a piezoelectric potential that promotes the separation and migration of charge carriers at the catalyst surface, thereby enabling pure water splitting. Pristine g-C_3N_4 exhibits an intrinsic piezoelectric response and can drive water splitting under ultrasonic stimulation; however, the generated piezoelectric potential and charge separation efficiency are relatively limited. Upon incorporation of Sn-based species into the g-C_3N_4 matrix, the piezoelectric potential is significantly enhanced due to interfacial coupling and strain amplification effects. The strengthened internal electric field accelerates charge transfer and suppresses carrier recombination, ultimately resulting in markedly improved piezocatalytic H_2 production.

To investigate the role of the piezoelectric effect in H_2O_2 production, the samples were evaluated in pure water under ultrasonication, without the addition of any sacrificial agents or cocatalysts. As shown in Fig. 4e, the H_2O_2 generation rates over two hours followed the order: M-0.5Sn > M-0.5Sn–N_2 ≥ M. Notably, M-

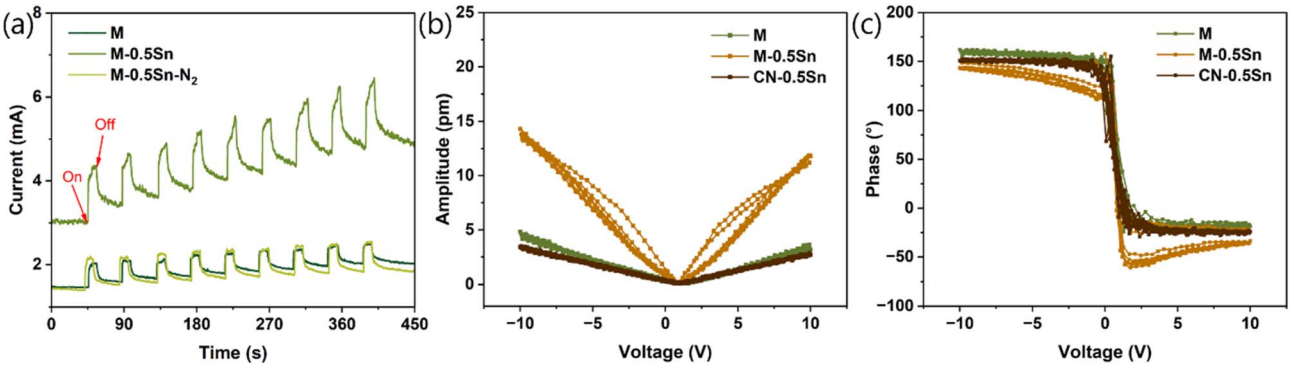

Fig. 5 (a) Piezo-current responses of M, M-0.5Sn, and M-0.5Sn–N_2, "On" means the time when ultrasonication was turn on, "Off" notes that the ultrasonication was turned off. The (b) phase and (c) amplitude hysteresis loops tested by piezo response force microscopy (PFM), for different samples.

0.5Sn achieved a production rate of 999.11 μmol g^{-1}, representing a nearly 14-fold increase compared to M (72.03 μmol g^{-1}) and approximately 10 times higher than M-0.5Sn–N_2 (99.22 μmol g^{-1}) within one hour. Similarly, the amount of $SnCl_2$ added during catalyst synthesis should have an optimal value, as M-0.5Sn shows the best performance compared to M-0.25Sn and M-1.0Sn (Fig. 4f). To elucidate the underlying reaction mechanisms and identify the active species, the influence of atmospheric conditions (air *vs.* N_2) on H_2O_2 production was first examined.[36] As shown in Fig. S9, the H_2O_2 yield of M-0.5Sn was significantly higher under an air atmosphere than under N_2, indicating that O_2 from the air is the primary source of H_2O_2 *via* reduction. This suggested that the contribution of water oxidation to H_2O_2 production is minimal during the piezocatalytic reaction. Subsequently, radical scavenging experiments were conducted using isopropyl alcohol (IPA) and benzoquinone (BQ) to probe the roles of hydroxyl radicals (*OH) and superoxide radicals ($*O_2^-$), respectively.[37] As illustrated in Fig. S9, the addition of BQ led to a marked suppression of H_2O_2 generation, implying that $*O_2^-$ is a key intermediate in the piezocatalytic process. In contrast, the presence of IPA had a negligible effect on H_2O_2 production, suggesting that *OH radicals are not significantly involved in the reaction pathway. Based on these findings, we propose that under ultrasonication, M-0.5Sn facilitates H_2O_2 production *via* a two-electron oxygen reduction pathway: adsorbed O_2 is reduced by piezoelectrically generated electrons to form $*O_2^-$, which is subsequently reduced to yield H_2O_2.[38]

Conclusion

In this study, we successfully introduced $SnCl_2$ as a molten salt medium for the synthesis of carbon nitride/metal oxide-based composites, demonstrating a simple yet highly effective strategy to engineer multifunctional piezocatalytic materials. The utilization of $SnCl_2$ under air atmosphere conditions played a critical dual role: it facilitated the thermal exfoliation of bulk graphitic carbon nitride into thinner nanosheets and promoted the formation and anchoring of oxidized Sn-based species onto the g-C_3N_4 framework. This process also led to the generation of structural defects within the carbon nitride matrix, which are known to enhance charge separation and active site availability. Remarkably, the prepared composites exhibited efficient dual-functional activity for H_2 and H_2O_2 production under ultrasonication, without using any sacrificial agents or additional co-catalysts. The observed enhancements are attributed to the modulation of the local electric field *via* the piezoelectric effect, which is believed to be strengthened by the $SnCl_2$ melt treatment in an oxidative environment. With optimized $SnCl_2$ loading, the composites achieved a notably high hydrogen evolution rate of 3846.46 μmol g^{-1} h^{-1}, alongside an impressive hydrogen peroxide production rate of 999.11 μmol g^{-1} h^{-1}. This work proves the potential of utilizing g-C_3N_4/metal oxide-based composites for the production of green energy and chemicals *via* mechanical energy.

Author contributions

Ying Pan: conceptualization, data curation, formal analysis, investigation, visualization, methodology, and writing. Luocheng Liao and Yunya Liu: piezoelectric effect testing and data analysis. Dan Qiao: H_2O_2 quantification. Irene Lamata Bermejo: XRD measurement. Ran Su: data curation, resources, and formal analysis. Nieves Lopez Salas: formal analysis, visualization, and resources. All authors contributed to discussions and commented on the manuscript, and all authors reviewed the manuscript.

Conflicts of interest

There are no conflicts to declare.

Data availability

Should any raw data files be needed in another format, they are available from the corresponding author upon reasonable request. Source data are provided with this paper.

The authors declare that the data supporting the findings of this study are available within the paper and its supplementary information (SI). Supplementary information: experimental details, characterization data, performance tests, and comparative table. See DOI: https://doi.org/10.1039/d5ta07919e.

Acknowledgements

Ying Pan acknowledges the financial support from the Postdoctoral Fellowship of the University of Paderborn. Nieves Lopez Salas acknowledges funding from DAAD Afriger project (577030859) and Fonds der Chemischen Industrie. Yunya Liu acknowledges funding from the Science and Technology Innovation Program of Hunan Province (2024RC3161). Ran Su acknowledges funding from the Natural Science Foundation of Hebei Province (E2019208243). The authors greatly acknowledge Alexandra Glas for carrying out the XPS measurement on sample M-0.5Sn in Fig. S7.

Notes and references

1 Q. Qian, Y. Zhu, N. Ahmad, Y. Feng, H. Zhang, M. Cheng, H. Liu, C. Xiao, G. Zhang and Y. Xie, Recent Advancements in Electrochemical Hydrogen Production *via* Hybrid Water Splitting, *Adv. Mater.*, 2024, **36**, 1–37, DOI: 10.1002/adma.202306108.

2 S. Fukuzumi, Y. M. Lee and W. Nam, Recent progress in production and usage of hydrogen peroxide, *Chin. J. Catal.*, 2021, **42**, 1241–1252, DOI: 10.1016/S1872-2067(20)63767-6.

3 R. Su, H. A. Hsain, M. Wu, D. Zhang, X. Hu, Z. Wang, X. Wang, F. Li, X. Chen, L. Zhu, Y. Yang, Y. Yang, X. Lou and S. J. Pennycook, Nano-Ferroelectric for High Efficiency Overall Water Splitting under Ultrasonic Vibration, *Angew. Chem.*, 2019, **131**, 15220–15225, DOI: 10.1002/ange.201907695.

4 R. Su, J. Zhang, V. Wong, D. Zhang, Y. Yang, Z. D. Luo, X. Wang, H. Wen, Y. Liu, J. Seidel, X. Yang, Y. Pan and F. tang Li, Engineering Sub-Nanometer Hafnia-Based Ferroelectrics to Break the Scaling Relation for High-

Efficiency Piezocatalytic Water Splitting, *Adv. Mater.*, 2023, **35**, 1–10, DOI: 10.1002/adma.202303018.

5 K. S. Hong, H. Xu, H. Konishi and X. Li, Direct water splitting through vibrating piezoelectric microfibers in water, *J. Phys. Chem. Lett.*, 2010, **1**, 997–1002, DOI: 10.1021/jz100027t.

6 R. Su, Z. Wang, L. Zhu, Y. Pan, D. Zhang, H. Wen, Z. D. Luo, L. Li, F. Tang Li, M. Wu, L. He, P. Sharma and J. Seidel, Strain-Engineered Nano-Ferroelectrics for High-Efficiency Piezocatalytic Overall Water Splitting, *Angew. Chem., Int. Ed.*, 2021, **60**, 16019–16026, DOI: 10.1002/anie.202103112.

7 S. Li, Z. Zhao, D. Yu, J. Z. Zhao, Y. Su, Y. Liu, Y. Lin, W. Liu, H. Xu and Z. Zhang, Few-layer transition metal dichalcogenides (MoS_2, WS_2, and WSe_2) for water splitting and degradation of organic pollutants: Understanding the piezocatalytic effect, *Nano Energy*, 2019, **66**, 104083, DOI: 10.1016/j.nanoen.2019.104083.

8 J. Xu, H. Che, C. Tang, B. Liu and Y. Ao, Tandem Fields Facilitating Directional Carrier Migration in Van der Waals Heterojunction for Efficient Overall Piezo-Synthesis of H_2O_2, *Adv. Mater.*, 2024, **36**, 1–9, DOI: 10.1002/adma.202404539.

9 H. Zeng, C. Liu, B. Lan, M. Tan, C. Yu, Y. Su, L. Qiao and Y. Bai, Bifunctional Bi0.98Sm0.02FeO_3/-C_3N_4 Piezocatalyst for Simultaneous H_2 and H_2O_2 Production, *ACS Appl. Mater. Interfaces*, 2024, **16**, 70566–70574, DOI: 10.1021/acsami.4c15127.

10 Y. Zheng, Y. Jia, H. Li, Z. Wu and X. Dong, Enhanced piezo-electro-chemical coupling of $BaTiO_3$/g-C_3N_4 nanocomposite for vibration-catalysis, *J. Mater. Sci.*, 2020, **55**, 14787–14797, DOI: 10.1007/s10853-020-05001-x.

11 W. Li, W. Duan, G. Liao, F. Gao, Y. Wang, R. Cui, J. Zhao and C. Wang, 0.68% of Solar-To-Hydrogen Efficiency and High Photostability of Organic-Inorganic Membrane Catalyst, *Nat. Commun.*, 2024, **15**, 6763, DOI: 10.1038/s41467-024-51183-2.

12 T. Ma, G. Liao, F. Gao, W. Duan, Y. Wang, R. Cui, C. Wang and W. Li, Flexible Hybrid Membrane with Synergistic Exciton Dynamics for Excessive 280 h of Durably Piezo-Photocatalytic H_2O-to-H_2 Conversion, *Small*, 2024, **20**, 1–12, DOI: 10.1002/smll.202408056.

13 S. Li, Z. Zhao, J. Zhao, Z. Zhang, X. Li and J. Zhang, Recent Advances of Ferro-, Piezo-, and Pyroelectric Nanomaterials for Catalytic Applications, *ACS Appl. Nano Mater.*, 2020, **3**, 1063–1079, DOI: 10.1021/acsanm.0c00039.

14 J. Ma, C. Peng, X. Peng, S. Liang, Z. Zhou, K. Wu, R. Chen, S. Liu, Y. Shen, H. Ma and Y. Zhang, H_2O_2 Photosynthesis from H_2O and O_2 under Weak Light by Carbon Nitrides with the Piezoelectric Effect, *J. Am. Chem. Soc.*, 2024, **146**, 21147–21159, DOI: 10.1021/jacs.4c07170.

15 M. Zelisko, Y. Hanlumyuang, S. Yang, Y. Liu, C. Lei, J. Li, P. M. Ajayan and P. Sharma, Anomalous piezoelectricity in two-dimensional graphene nitride nanosheets, *Nat. Commun.*, 2014, **5**, 4284, DOI: 10.1038/ncomms5284.

16 Z. Li, Y. Zhou, Y. Zhou, K. Wang, Y. Yun, S. Chen, W. Jiao, L. Chen, B. Zou and M. Zhu, Dipole field in nitrogen-enriched carbon nitride with external forces to boost the artificial photosynthesis of hydrogen peroxide, *Nat. Commun.*, 2023, **14**, 5742, DOI: 10.1038/s41467-023-41522-0.

17 J. Barrio, M. Volokh and M. Shalom, Polymeric carbon nitrides and related metal-free materials for energy and environmental applications, *J. Mater. Chem. A*, 2020, **8**, 11075–11116, DOI: 10.1039/d0ta01973a.

18 K. Wang, D. Shao, L. Zhang, Y. Zhou, H. Wang and W. Wang, Efficient piezo-catalytic hydrogen peroxide production from water and oxygen over graphitic carbon nitride, *J. Mater. Chem. A*, 2019, **7**, 20383–20389, DOI: 10.1039/c9ta06251c.

19 N. Rono, J. K. Kibet, B. S. Martincigh and V. O. Nyamori, A comparative study between thermal etching and liquid exfoliation of bulk graphitic carbon nitride to nanosheets for the photocatalytic degradation of a model environmental pollutant, Rhodamine B, *J. Mater. Sci.: Mater. Electron.*, 2021, **32**, 687–706, DOI: 10.1007/s10854-020-04849-8.

20 J. Kossmann, T. Heil, M. Antonietti and N. López-Salas, Guanine-Derived Porous Carbonaceous Materials: Towards C1N1, *ChemSusChem*, 2020, **13**, 6643–6650, DOI: 10.1002/cssc.202002274.

21 Z. Pan, M. Zhao, H. Zhuzhang, G. Zhang, M. Anpo and X. Wang, Gradient Zn-doped poly heptazine imides integrated with a van der Waals homojunction boosting visible light-driven water oxidation activities, *ACS Catal.*, 2021, **11**, 13463–13471, DOI: 10.1021/acscatal.1c03687.

22 M. Cao, K. Wang, I. Tudela and X. Fan, Synthesis of Zn doped g-C_3N_4 in KCl-$ZnCl_2$ molten salts: The temperature window for promoting the photocatalytic activity, *Appl. Surf. Sci.*, 2020, **533**, 147429, DOI: 10.1016/j.apsusc.2020.147429.

23 X. Zheng, Z. Tian, R. Bouchal, M. Antonietti, N. López-Salas and M. Odziomek, Tin (II) Chloride Salt Melts as Non-Innocent Solvents for the Synthesis of Low-Temperature Nanoporous Oxo-Carbons for Nitrate Electrochemical Hydrogenation, *Adv. Mater.*, 2024, **36**, 1–12, DOI: 10.1002/adma.202311575.

24 S. Yang, Y. Gong, J. Zhang, L. Zhan, L. Ma, Z. Fang, R. Vajtai, X. Wang and P. M. Ajayan, Exfoliated graphitic carbon nitride nanosheets as efficient catalysts for hydrogen evolution under visible light, *Adv. Mater.*, 2013, **25**, 2452–2456, DOI: 10.1002/adma.201204453.

25 J. Zhang, X. Liang, C. Zhang, L. Lin, W. Xing, Z. Yu, G. Zhang and X. Wang, Improved Charge Separation in Poly(heptazine-triazine) Imides with Semi-coherent Interfaces for Photocatalytic Hydrogen Evolution, *Angew. Chem., Int. Ed.*, 2022, **61**, e20221084, DOI: 10.1002/anie.202210849.

26 S. Ganesan, T. Kokulnathan, S. Sumathi and A. Palaniappan, Efficient photocatalytic degradation of textile dye pollutants using thermally exfoliated graphitic carbon nitride (TE-g-C_3N_4), *Sci. Rep.*, 2024, **14**, 2284, DOI: 10.1038/s41598-024-52688-y.

27 L. Yang, J. Huang, L. Shi, L. Cao, Q. Yu, Y. Jie, J. Fei, H. Ouyang and J. Ye, A surface modification resultant thermally oxidized porous g-C3N4 with enhanced photocatalytic hydrogen production, *Appl. Catal., B*, 2017, **204**, 335–345, DOI: 10.1016/j.apcatb.2016.11.047.

28 A. R. Kamali, G. Divitini, C. Ducati and D. J. Fray, Transformation of molten $SnCl_2$ to SnO_2 nano-single

crystals, *Ceram. Int.*, 2014, **40**, 8533–8538, DOI: 10.1016/j.ceramint.2014.01.067.

29 S. Panja, Y. Miao, J. Döhn, J. Choi, S. Fleischmann, S. Guddehalli Chandrappa, T. Diemant, A. Groß, G. Karkera and M. Fichtner, Synthesis, Structural Analysis, and Degradation Behavior of Potassium Tin Chloride as Chloride-Ion Batteries Conversion Electrode Material, *Adv. Funct. Mater.*, 2024, **35**, 2413489, DOI: 10.1002/adfm.202413489.

30 Z. Li, K. Tong, H. Dong, Y. Li, K. Wang, T. Ding, Y. Yun, Y. Zhou and M. Zhu, H-Bonds in Carbon Quantum Dot-anchored C_3N_5 to Boost Proton-Coupled Electron Transfer for Piezoelectric-Driven Hydrogen Peroxide Synthesis under Ambient Conditions, *Angew. Chem., Int. Ed.*, 2025, **64**, e202502390, DOI: 10.1002/anie.202502390.

31 Q. Deng, H. Li, W. Hu and W. Hou, Stability and Crystallinity of Sodium Poly(Heptazine Imide) in Photocatalysis, *Angew. Chem., Int. Ed.*, 2023, **62**, e202314213, DOI: 10.1002/anie.202314213.

32 W. Wang, H. Zhang, S. Zhang, Y. Liu, G. Wang, C. Sun and H. Zhao, Potassium-Ion-Assisted Regeneration of Active Cyano Groups in Carbon Nitride Nanoribbons: Visible-Light-Driven Photocatalytic Nitrogen Reduction, *Angew. Chem., Int. Ed.*, 2019, **58**, 16644–16650, DOI: 10.1002/anie.201908640.

33 M. Kwoka, L. Ottaviano, M. Passacantando, S. Santucci, G. Czempik and J. Szuber, XPS study of the surface chemistry of L-CVD SnO_2 thin films after oxidation, *Thin Solid Films*, 2005, **490**, 36–42, DOI: 10.1016/j.tsf.2005.04.014.

34 A. Y. Mohamed, S. J. Lee, Y. Jang, J. S. Kim, C. S. Hwang and D. Y. Cho, X-ray spectroscopy study on the electronic structure of Sn-added p-type SnO films, *J. Condens. Matter Phys.*, 2020, **32**, 065502, DOI: 10.1088/1361-648X/ab4f51.

35 R. Li, G. Zhang, Y. Wang, Z. Lin, C. He, Y. Li, X. Ren, P. Zhang and H. Mi, Fast ion diffusion kinetics based on ferroelectric and piezoelectric effect of $SnO_2/BaTiO_3$ heterostructures for high-rate sodium storage, *Nano Energy*, 2021, **90**, 106591, DOI: 10.1016/j.nanoen.2021.106591.

36 H. Yang, C. Li, T. Liu, T. Fellowes, S. Y. Chong, L. Catalano, M. Bahri, W. Zhang, Y. Xu, L. Liu, W. Zhao, A. M. Gardner, R. Clowes, N. D. Browning, X. Li, A. J. Cowan and A. I. Cooper, Packing-induced selectivity switching in molecular nanoparticle photocatalysts for hydrogen and hydrogen peroxide production, *Nat. Nanotechnol.*, 2023, **18**, 307–315, DOI: 10.1038/s41565-022-01289-9.

37 Q. Wu, J. Cao, X. Wang, Y. Liu, Y. Zhao, H. Wang, Y. Liu, H. Huang, F. Liao, M. Shao and Z. Kang, A metal-free photocatalyst for highly efficient hydrogen peroxide photoproduction in real seawater, *Nat. Commun.*, 2021, **12**, 483, DOI: 10.1038/s41467-020-20823-8.

38 W. Zhao, P. Yan, B. Li, M. Bahri, L. Liu, X. Zhou, R. Clowes, N. D. Browning, Y. Wu, J. W. Ward and A. I. Cooper, Accelerated Synthesis and Discovery of Covalent Organic Framework Photocatalysts for Hydrogen Peroxide Production, *J. Am. Chem. Soc.*, 2022, **144**, 9902–9909, DOI: 10.1021/jacs.2c02666.